NASA
Technical
Paper
2896

1989

Measured and Predicted Root-Mean-Square Errors in Square and Triangular Antenna Mesh Facets

W. B. Fichter
Langley Research Center
Hampton, Virginia

National Aeronautics and
Space Administration
Office of Management
Scientific and Technical
Information Division

Summary

Deflection shapes of square and equilateral-triangular facets of two tricot-knit, gold-plated, molybdenum wire-mesh antenna materials were measured and compared, on the basis of root-mean-square (rms) differences, with deflection shapes predicted by linear membrane theory for several cases of biaxial mesh tension. The two mesh materials contained approximately 10 and 16 holes per lineal inch, measured diagonally with respect to the course and wale directions. The deflection measurement system employed a noncontact eddy-current proximity probe and an electromagnetic distance-sensing probe in conjunction with a precision optical level. Despite experimental uncertainties, rms differences between measured and predicted deflection shapes suggest the following conclusions: (1) replacing flat antenna facets with facets that conform to parabolically curved structural members yields smaller rms surface error; (2) accuracy gains are potentially greater for equilateral-triangular facets than for square facets; (3) linear membrane theory can be a useful tool in the design of tricot-knit wire-mesh antennas.

Introduction

In reference 1, the potential for reducing root-mean-square (rms) surface error in shallow faceted reflectors is examined by replacing flat facets with laterally curved membrane facets (i.e., facets whose lateral deflections were assumed to be governed by linear membrane theory). Exact solutions were obtained for the small lateral deflections of rectangular and equilateral-triangular membranes subject to isotropic tension and parabolic edge deflections. These solutions were used to minimize the rms error between a facet of a shallow paraboloidal reflector and its approximating membrane facet. The resulting optimum placements and edge curvatures yielded membrane facets that had significantly smaller rms errors than the corresponding best-fit flat facets. These results suggested that replacement of flat facets with membrane facets that conform to curved structural members could produce reflectors with lower rms error, or comparable error with larger facets and, hence, fewer structural members.

This promising conclusion from reference 1 is predicated on the assumption that the reflector material deforms according to linear membrane theory. This paper reports on a combined experimental and analytical study to test the assumption. The experimental portion consisted of subjecting two different samples of tricot-knit metallic mesh material to various known tension fields, imposing known parabolic deflection along square and equilateral-triangular test-section boundaries, and measuring the resulting mesh deflection shapes within the boundaries. The analytical portion consisted of obtaining membrane solutions that included gravity loading and, for rectangular membranes, unequal biaxial tensions. These solutions were used along with solutions from reference 1 to compare measured with predicted deflections on the basis of rms differences.

Symbols

A	area of triangle
a	half-length of rectangle
b	half-width of rectangle
h	rigid body translation used in minimizing mean-square difference
i	integer
L	length of equilateral-triangle edge
n	integer
p	weight of mesh per unit area
R	minimum radius of curvature of parabolic edge
T	mesh tension force per unit length
W	maximum edge deflection
w	mesh or membrane deflection
x,y	rectangular Cartesian coordinates
$z(x,y)$	paraboloidal shape function
γ	parameter defined in the appendix
δ_F	rms difference between ideal paraboloid and best-fit flat facet
δ_M	rms difference between ideal paraboloid and congruent-edge membrane
δ_1	rms difference between measured and predicted deflections
δ_2	rms difference between measured shape and best-fit paraboloid

Experiments

Test Specimens

Closeup views of the two mesh materials tested are shown in figure 1. Both were tricot knits of gold-plated molybdenum wire which was nominally 1 mil in diameter. Geometrically, the meshes differed in the density of the knit; the coarse mesh had about 10 holes per inch, and the fine mesh had about

16 holes per inch, measured diagonally with respect to the course and wale directions. When prepared for the tests, both specimens were about 3 ft square. This size was assumed to be large enough to allow the tensioning forces applied at 1-in. intervals along all edges to diffuse to essential uniformity in two orthogonal directions inside the square and triangular test sections located near the center of the specimens. The square test section was 16 in. on a side, and the triangular test section was 18 in. on a side. Care was taken to obtain mesh samples that were free of visible flaws such as creases in the fabric or breaks in individual wires, especially in or near the test sections. Also, to prevent unacceptable permanent out-of-plane deformation of the mesh materials, considerable care was exercised in handling them for any purpose (e.g., measuring and cutting, tensioning, and installing or removing specimens from the tensioning frame). Areal densities of the two mesh materials, which were required for calculations of gravity-induced deflections, were estimated by putting mesh samples under light biaxial tension, marking and cutting 1-ft-square sections, and weighing them on a chemical balance. Densities obtained were 3.4×10^{-5} and 4.8×10^{-5} lb/in^2 for the coarse and fine meshes, respectively.

Test Setup and Instrumentation

An overall view of the test setup is shown in figure 2. To produce the desired average mesh tensions in two orthogonal directions, 0.01-lb removable split shot were pressed onto lengths of lightweight monofilament line, which were then hooked onto the edges of the mesh by use of appropriately reshaped standard office staples attached to the lines. Initially, a 3-ft-square mesh sample was spread out on a portable tensioning board and a few weights were hung at relatively large intervals along each edge. The mesh was then transferred to the tensioning frame shown in figure 2 by lowering the tensioning board through the frame while guiding the weights over the sides of the frame. After the mesh was suspended horizontally, more weights were hung, until they were spaced at 1-in. intervals on all four edges. From this point on, average tension in either direction was altered, as required, in 0.01-lb/in. increments by adding or removing split shot.

The mesh-tensioning frame was a square framework of four 1/4-in-diameter steel rods covered with Teflon tape to reduce friction between the rods and the monofilament lines. Supporting the frame were four vertical 3/4-in-diameter steel posts on magnetic bases. A 5-ft-square, 3-in-thick, steel testing-machine platen provided a stable platform for the test setup.

Also mounted on the posts (after mounting of a mesh specimen) was a four-armed radial frame of 3/4-in-diameter steel tubes with a hub that accommodated a vertical steel tube. This tube supported the square and triangular "shaping" frames which, when lowered just enough to effect all-round contact with the mesh, imposed parabolic lateral deflections along the edges of the shaping frame.

The shaping frames consisted of 1/2-in-thick rails of a dielectric material; these rails were flat on the upper surface and the lower surface was shaped on a numerical-control milling machine. Lengthwise, each rail lower surface profile was parabolic with a nominal 0.25-in. rise and was symmetric about its midlength. Across the rail thickness, each lower surface profile was a half circle. The minimum height of each rail (at the vertices of the square and rectangle) was 1 in., which was hence the minimum distance between the mesh and the 1/2-in-thick aluminum backing plate of the shaping frames. The lower rail surfaces, the only areas of contact between the mesh and the shaping frames, were given a smooth finish to minimize friction between the mesh and the rails. The lower surface of each backing plate had been machined as near to flat as practicable to provide a plane of reference for the rail-induced mesh deflections.

The base for the instruments used to measure mesh deflections was a surveyor that was nominally designed for ultrasonic scanning of material systems. The surveyor consisted of a rectangular tank with two longitudinal rails on which rode a screw-driven transverse beam. Affixed to the transverse beam was a belt-driven carriage on which the deflection-measuring instruments were mounted. The carriage could be moved, in a nominal horizontal plane, to any desired location within approximately a 20-in. by 24-in. rectangular test region. Although motorized operation was possible, the carriage was always translated by hand cranking for more precise control of translation speed and location.

The deflection-measuring instruments mounted on the carriage consisted of a 3/8-in-diameter, noncontact, mesh-sensing probe, a motor for vertically translating the probe as required, and an instrument for measuring the vertical translation of the probe relative to a fixed point on the carriage. (See fig. 3.) As it is traditionally used, the probe detects its distance from the mesh by sensing eddy currents induced in the mesh by current flow in the probe. A previously established nonlinear calibration curve is then used to obtain separation distance at each point where probe voltage is read and, thus, a map of the mesh surface deflections relative to the plane in which the probe operates. In the present tests, however, the nonlinear calibration curve of the probe was not required because a feedback control system was employed which sensed the probe voltage and commanded the motor to move the probe vertically as required to maintain a preset constant probe voltage and, hence, a constant distance between probe and mesh. An electromagnetic distance-measuring instrument attached to the carriage, with its target mounted on the probe shaft (which translated with the probe), gave readings of the vertical translation of the probe (hence, the mesh) relative to the carriage. In each test, simultaneous x, y, and z readings were made at the vertices of the shaping frames and at 64 uniformly distributed interior points; the x and y readings were made by using linear potentiometers built into the surveyor.

A horizontal plane which served as a datum for all vertical measurements was defined by an optical level. With a target mounted on the carriage, the optical level also facilitated corrections to the data for vertical translations of the carriage. (Early in the experimental program it was determined that the carriage did not move in a plane.) During a test, x, y, and z readings were made at each station, the z readings were corrected for vertical displacement of the carriage, and the data were recorded and printed, after which the carriage was translated to the next station in the test sequence.

Typical Test

First, each side of the mesh-tensioning frame was rapped lightly several times to minimize static-friction forces between the mesh and the rails and/or the tensioning frame. One rail of the shaping frame was then aligned parallel with the longitudinal axis of the surveyor, and potentiometer voltages were adjusted for the proper x and y zeros and total excursions. Readings at each vertex were then taken, corrected (z only), and recorded. These vertex readings facilitated correction of the vertical displacement data for the tilt of the shaping frame relative to a horizontal reference plane. Readings were then taken sequentially at the 64 uniformly distributed stations inside the shaping frame; these readings completed a test. If a scan of the printed data revealed no anomalies, the entire data-taking sequence was repeated to produce full data sets for two nominally identical tests. Split shot were then added or removed to change the biaxial tension in preparation for the next pair of tests with the same mesh and shaping-frame combination.

Although x- and y-translations of the probe carriage could have been performed by electric motors built into the surveyor, they were effected by hand cranking for more precise control of translation speed and location. This was done with the aid of station-by-station instructions displayed on the computer used to correct and store data and with x and y location-related voltages displayed on two digital voltmeters. To assure that probe voltage remained constant throughout a test, it was monitored with a third digital voltmeter. At each station in the test sequence, the probe carriage was stopped and x, y, and z data were taken, corrected (z only), and printed before translation to the next station was begun. Locations x and y, at which data were taken, are indicated by the numbered dots in figure 4.

Analysis and Data Correlation

Membrane Solutions

In reference 1, solutions were obtained for isotropically tensioned rectangular and equilateral-triangular membranes with parabolic deflections imposed on all boundaries. Use of these solutions in the present study required their modification to account for gravity-induced deflections. Also, the rectangular membrane solution has been generalized to the case of unequal biaxial tensions. (A similar generalization was sought for the triangular membrane, but without success.) Details are given in the appendix. The membrane solutions used herein are summarized below. (See fig. 4 for coordinate systems and notation.)

Square. For the square membrane with edges of length $2a$ and areal density p, subjected to uniform tensions T_x and T_y, and with boundary conditions $w(x, \pm a) = W\left(1 - \frac{x^2}{a^2}\right)$ and $w(\pm a, y) = W\left(1 - \frac{y^2}{a^2}\right)$, the deflection shape is given by

$$w(x,y) = w_r(x,y) + w_g(x,y) \tag{1}$$

where w_r, the deflection due to the rail-induced edge displacements, is defined by

$$w_r(x,y) = \frac{32W}{\pi^3} \sum_{n\,\mathrm{odd}}^{\infty} \frac{(-1)^{\frac{n-1}{2}}}{n^3} \times \left[\frac{\cos\left(\frac{n\pi x}{2a}\right)\cosh\left(\frac{n\pi\gamma y}{2a}\right)}{\cosh\left(\frac{n\pi\gamma}{2}\right)} + \frac{\cosh\left(\frac{n\pi x}{2\gamma a}\right)\cos\left(\frac{n\pi y}{2a}\right)}{\cosh\left(\frac{n\pi}{2\gamma}\right)} \right] \tag{2}$$

and w_g, the additional deflection due to gravity loading, is defined by

$$w_g(x,y) = \frac{16a^2p}{\pi^3 T_x} \sum_{n\,\mathrm{odd}}^{\infty} \frac{(-1)^{\frac{n-1}{2}}}{n^3}$$

$$\times \left[1 - \frac{\cosh\left(\frac{n\pi\gamma y}{2a}\right)}{\cosh\left(\frac{n\pi\gamma}{2}\right)}\right] \cos\left(\frac{n\pi x}{2a}\right) \qquad (3)$$

and, for the square, $\gamma^2 = \frac{T_x}{T_y}$. (Note that $w = 0$ at all vertices.)

Triangle. For the equilateral-triangular membrane with edges of length L, areal density p, isotropic tension T, and identical symmetric parabolic deflections on the three edges—for example,

$$w\left(\frac{\sqrt{3}}{6}L, y\right) = W\left(1 - 4\frac{y^2}{L^2}\right)$$

the deflection shape is

$$w(x,y) = W\left[\frac{8}{9} + \frac{4}{9}\lambda - 4\lambda\left(\frac{x^2}{L^2} + \frac{y^2}{L^2}\right)\right.$$

$$\left. + (1-\lambda)\frac{8\sqrt{3}}{3}\frac{x}{L}\left(\frac{x^2}{L^2} - 3\frac{y^2}{L^2}\right)\right] \qquad (4)$$

where $\lambda = \frac{pR}{2T}$. (Again, $w = 0$ at all vertices.)

Differences Between Measured and Predicted Shapes

For each test, the rms difference δ_1 between the measured deflections $w_m(x,y)$ and the deflections predicted by linear membrane theory $w(x,y)$ was calculated from

$$\delta_1^2 = \frac{1}{64}\sum_{i=1}^{64}\left[w_m(x_i,y_i) - w(x_i,y_i)\right]^2 \qquad (5)$$

where i denotes the station number. The theoretical deflection $w(x,y)$ is given by equations (1) to (3) for the square and by equation (4) for the triangle. As the measured deflections $w_m(x,y)$ were recorded, they were automatically corrected for vertical excursions of the carriage on the basis of optical-level readings already made at each station.

The measured deflections also required correction because of the tilt of the shaping frame with respect to a horizontal plane. In the case of the triangle, z readings taken at the three vertices at the beginning of each test were used to define a plane with the equation

$$w_c(x,y) = c_0 + c_1 x + c_2 y$$

In the case of the square, the four vertex z readings were used to define a least-squares best-fit plane with the equation

$$w_c(x,y) = c_0 + c_1 x + c_2 y$$

Corrections calculated for each station from these equations were subtracted from the measured deflections before their insertion into equation (5). Adequate numbers of terms were retained in the series in equations (2) and (3) to ensure good convergence. Of course, no such truncation was required for the purely algebraic deflection function of the triangle.

Differences Between Measured and Ideal Shapes

Another comparison of interest is between the measured surface and the paraboloidal facet which has the edge deflections of the shaping frame and which best fits the measured surface in the least-squares sense. The shape of the best-fit paraboloid is fully specified by the shaping frame; this leaves only the determination of the vertical rigid-body translation that places the paraboloid in the minimum mean-square error position. This translation is found by adding an undetermined vertical component h to the paraboloid shape function and then solving for h in each case by minimizing, with respect to h, the resulting mean-square difference between the measured and ideal shapes. This value is then substituted into the mean-square error expression to obtain the rms difference between each measured shape and its best-fit paraboloid.

Thus, with the mean-square error defined by

$$\delta_2^2 = \frac{1}{64}\sum_{i=1}^{64}\left[h + z(x_i,y_i) - w_m(x_i,y_i)\right]^2 \qquad (6)$$

where $z(x,y)$ is the shape function for the paraboloid, the optimum value of h is determined by

$$\frac{d}{dh}\left(\delta_2^2\right) = 0$$

which yields

$$h = -\frac{1}{64}\sum_{i=1}^{64}\left[z(x_i,y_i) - w_m(x_i,y_i)\right] \qquad (7)$$

For each set of measurements $w_m(x,y)$ a value of h is computed and then inserted, along with $w_m(x,y)$, into equation (6) to obtain the rms difference between the measured surface and its best-fit paraboloid.

Results and Discussion

Experimental Accuracy

Before computations of rms differences based on test measurements are presented, some comments on experimental accuracy are in order. Potential sources of uncertainty in mesh-deflection measurements are as follows:

1. Noncontact mesh-sensing probe
2. Electromagnetic instrument used to measure vertical excursions of the probe relative to the probe carrier
3. Numerically machined dielectric rails of the shaping frame
4. Nonplanarity of the shaping-frame backing plate
5. Nonplanar motions of the probe carrier and the use of an optical level to account for them
6. Determination of the locations of the shaping-frame vertices, that is, the vertices of the square and triangular mesh facets
7. Mesh irregularities and areal density measurements

On the basis of manufacturers' specifications and in-house calibration tests, the combined uncertainties in readings from the mesh-sensing probe and the electromagnetic distance-measuring instrument should be on the order of ±0.001 in.

Although the rails of the shaping frame were intended to have a parabolic longitudinal profile with a vertex-to-midlength excursion of 0.250 in., micrometer measurements yielded values of 0.245 (±0.002) in. for the square, and 0.246 (±0.002) in. for the triangle. The average measured values were used in all calculations.

After the lower surface of the backing plate of each shaping frame was machined as near to flat as practicable, measurements were made at numerous points near the dielectric rails. Out-of-plane deviations were found to be in the ranges of ±0.001 in. for the square and ±0.002 in. for the triangle. Because of their random nature and uncertainty about their effect on rail profiles, no attempt was made to account for these backing-plate inaccuracies.

The nonplanar probe-carrier excursions and corrections for them by use of an optical level probably constitute one of the most significant sources of error. Although the optical level could be read to within about 0.0005 in., repeatability of sightings on a fixed target was probably no better than ±0.002 in.

Properly accounting for tilt of the shaping frames required accurate readings of the height of each vertex. Thus, variances in repeatability could be expected to result in similar variances in the rms difference calculations. Also, repeatedly positioning the probe precisely under each vertex left little margin for error, because mesh displacement gradients, although quite gentle inside the test section, were relatively steep immediately outside the boundaries. Though absolute limits are not known, rough calculations based on the test procedure suggest that uncertainties on the order of ±0.002 in. in vertex height measurements are possible.

Mesh irregularities which could contaminate the data fall into two categories: visible flaws, such as broken wires or creases in the fabric, and nonuniform electrical conductivity. Care was taken to obtain and prepare mesh specimens with no visible flaws in or near the test sections, and, in fact, no such flaws were detected. Information on nonuniform mesh conductivity, which might lead to nonuniform probe response, appears to be scant. It is known, however, that oxidation of the wire surface can degrade mesh conductivity; hence, nonuniform oxidation of a mesh specimen might translate into nonuniform probe response. Also, while the fine mesh was tested within a few weeks of manufacture, the coarse mesh is known to have spent several months in a nonideal environment prior to testing.

In addition to the potential sources of experimental error, there is also the discretization effect associated with using a finite number (64) of data points to represent the continuous membrane deflection shape. To obtain an estimate of the potential for discretization error, the following "worst-case" calculations were performed for the triangle:

$$s_e^2 = \frac{1}{A}\iint w^2 dA \qquad (exact)$$

and

$$s_d^2 = \frac{1}{64}\sum_1^{64} w_1^2 \qquad (discrete)$$

where

$$w = W\left[\frac{8}{9} + \frac{8\sqrt{3}}{3}\left(x^2 - 3y^2\right)\right]$$

is the deflection, measured from the plane containing the vertices, of a membrane with parabolic edge deflections, and $W = 0.246$ in. is the maximum edge deflection. To three significant figures,

$$s_e = \sqrt{\frac{2}{3}} W = 0.201 \text{ in.}$$

and

$$s_d = 0.201 \text{ in.}$$

These results indicate that discretization error was insignificant in the present study.

With all the potential sources of experimental uncertainty taken into account, it appears reasonable to conclude that the mesh deflection data may be accurate to no better than ±0.005 in., with most of the uncertainty caused by (1) out-of-plane excursions of the probe carrier and use of the optical level to account for them, and (2) difficulties in precisely and repeatedly positioning the mesh-sensing probe directly under each vertex of the square and triangle.

Root-Mean-Square Differences

Computations based on the experimental data are presented in tables 1 and 2 for the square and triangular facets, respectively. Values listed are for δ_1, the rms difference between measured and predicted shapes, and for δ_2, the rms difference between the measured shapes and their best-fit congruent-edge paraboloids, for several combinations of biaxial mesh tension. Consistent with possibly optimistic estimates of experimental accuracy, three decimal places are retained in computations of δ_1 and δ_2. Also listed for easy reference are values of δ_M, the rms difference between the ideal paraboloid and its best-fit congruent-edge membrane, and δ_F, the rms difference between the ideal paraboloid and its best-fit flat facet. (See ref. 1.)

Square-facet results. Root-mean-square difference calculations are presented for five biaxial tension combinations. The scatter in δ_1 for a particular combination of T_x and T_y is generally greater for the coarse mesh than for the fine mesh. One possible explanation for this is nonuniform probe response to the coarse mesh as a result of its greater oxidation, since the coarse mesh had been stored under nonideal conditions considerably longer before testing than had the fine mesh. On the other hand, the scatter in δ_2, the rms difference between the measured shapes and their best-fit paraboloids, is very small for both facet shapes. Of course, this could mean merely that, within some practical limits, paraboloids can be fit equally well to data sets of different accuracies.

For both meshes, δ_1 is generally much smaller than δ_2, in a few cases by nearly an order of magnitude. This difference suggested that, despite significant experimental uncertainty, linear membrane theory can be a useful predictive tool for square mesh facets for the geometrical parameters of the present study. Also, with one or two exceptions, a scan of the δ_1 column indicates a trend toward less accurate membrane theory predictions with increasing strength of the remote tension field. Such a trend would seem to be consistent with the growing importance of nonlinear membrane effects with increasing tension.

A comparison of δ_2 for both meshes with δ_M, the theoretical rms difference between the ideal paraboloid and its best-fit congruent-edge membrane, shows that, although they are of comparable magnitude, δ_2 is always smaller than δ_M. This difference suggests that an antenna design based on linear membrane theory is likely to be conservative, since the membrane theory consistently overestimated the rms difference between the mesh and the ideal surface for the range of parameters investigated. Also, δ_M is quite insensitive to T_x/T_y for $1 \leq T_x/Ty \leq 3$.

A comparison of δ_M values for the different T_x/T_y ratios with δ_F, the rms difference between the ideal paraboloid and its best-fit flat facet, reveals the meagerness of accuracy gains which are achievable by replacing square flat facets with congruent-edge membrane facets.This finding is consistent with analytical results from reference 1. In every case, the theoretical reduction in rms difference is less than 20 percent. This fact, along with the uninspiring values of $\delta_F = 0.1033$ in. for a 16-in-square facet, strongly suggests that subdividing a reflector surface into square facets is not an economical means of achieving high surface accuracy, since it would require relatively small facets and thus high part count and complexity.

Triangular-facet results and comparisons with square-facet results. Root-mean-square difference calculations are presented for three levels of equal biaxial tension. The scatter in δ_1 is generally smaller for the triangle than for the square, though the data set is probably too small to support any claims of a clear trend.

Again, δ_1 for each triangular mesh is smaller than δ_2. However, the differences between them are considerably smaller than for the square. Each of two phenomena probably account partially for these smaller differences. First, all the δ_2 values for the triangle are small compared with those for the square, which is consistent with the conclusion from reference 1 that triangular membrane facets can be made to fit the paraboloid better than can square facets of comparable size. This contention is supported by the δ_M calculations for the triangle and the square. Second, the fact that the δ_1 values for the triangle and the square are comparable may simply indicate that a significant part of δ_1 for both facets is the result of experimental uncertainties, rather than differences between predicted and actual mesh deflection shapes.

While the scatter in δ_2 is quite small for both meshes and both facet shapes, the δ_2 values are generally smaller for the fine mesh. This difference could be caused by the possibly greater oxidation of the coarse mesh, as mentioned previously. However, it could also suggest that the fine mesh conforms more closely to the ideal paraboloidal shape, whether or not it adheres more closely to linear membrane theory.

Concluding Remarks

Deflection measurements of both square and triangular facets of two tricot-knit, gold-plated, molybdenum wire-mesh materials under several biaxial tension fields and related rms difference calculations suggest, despite experimental uncertainties, that linear membrane theory can be a useful tool in the design of tricot-knit wire-mesh antennas. Calculated rms differences between measured deflection shapes and their best-fit congruent-edge paraboloids, while always comparable to rms differences predicted by linear membrane theory, were generally somewhat smaller (1 to 38 percent for the triangle, 12 to 34 percent for the square). This may indicate that an antenna design based on linear membrane theory could be more accurate than expected. However, a more definite conclusion would require a more extensive and refined experimental program.

Tricot knits, because of their relatively low inplane shear stiffness, would be expected to adhere more closely to membrane theory than would most other mesh materials. In fact, this was a major consideration in choosing the meshes to be tested. Thus, it is by no means certain that the tentative conclusions reached here about the applicability of linear membrane theory to tricot-knit meshes can be generalized to other mesh types. Any such extrapolation would need to be supported by appropriate test data.

The experimental program was designed to test the findings of linear analyses of membranes in biaxial and isotropic tension fields; hence, the numerical results are not expected to apply directly to any antenna design and fabrication effort that involves more complex tension fields. However, because linear membrane theory is generally well suited to numerical analysis methods, it might still be profitably employed when mesh tensions, although variable, are reasonably well-known.

Appendix

Some Solutions for Rectangular and Equilateral-Triangular Membranes

Accounting for gravity-induced contributions to the total mesh deflection requires modification of the membrane solutions obtained in reference 1. In the case of the rectangular membrane, the effects of unequal biaxial tensions are also easily included.

Rectangular Membrane

For constant biaxial tensions T_x and T_y and uniform lateral loading p, the partial differential equation governing the lateral deflection w is

$$T_x \frac{\partial^2 w}{\partial x^2} + T_y \frac{\partial^2 w}{\partial y^2} = -p \tag{A1}$$

If the boundaries of a rectangular membrane with sides of length $2a$ and $2b$ are required to be congruent with a paraboloid with the equation

$$z(x,y) = \frac{a^2+b^2}{2R} - \frac{x^2+y^2}{2R}$$

then the membrane boundary conditions are

$$w(\pm a, y) = \frac{b^2}{2R}\left(1 - \frac{y^2}{b^2}\right) \tag{A2}$$

and

$$w(x, \pm b) = \frac{a^2}{2R}\left(1 - \frac{x^2}{a^2}\right) \tag{A3}$$

Through symmetry considerations and superposition, the solution to the problem defined by equations (A1) to (A3) can be written as the sum of the solutions to three problems defined by equation (A1) and the following sets of boundary conditions:

I. $\frac{\partial w}{\partial x}(0,y) = w(a,y) = \frac{\partial w}{\partial y}(x,0) = 0$ and $w(x,b) = \frac{a^2}{2R}\left(1 - \frac{x^2}{a^2}\right)$, with $p = 0$ in equation (A1) (A4)

II. $\frac{\partial w}{\partial x}(0,y) = w(x,b) = \frac{\partial w}{\partial y}(x,0) = 0$ and $w(a,y) = \frac{b^2}{2R}\left(1 - \frac{y^2}{b^2}\right)$, with $p = 0$ in equation (A1) (A5)

III. $w(x,\pm b) = w(\pm a, y) = 0$, with $p \neq 0$ in equation (A1) (A6)

The Fourier series solution to problem I is

$$w_I(x,y) = \frac{32}{\pi^3}\left(\frac{a^2}{2R}\right) \sum_{n\,\mathrm{odd}}^{\infty} \frac{(-1)^{\frac{n-1}{2}}}{n^3} \left[\frac{\cos\left(\frac{n\pi x}{2a}\right)}{\cosh\left(\frac{n\pi\gamma}{2}\right)}\right] \cosh\left(\frac{n\pi\gamma y}{2b}\right) \tag{A7}$$

where $\gamma^2 = \frac{b^2}{a^2}\frac{T_x}{T_y}$. The solution to problem II is

$$w_{II}(x,y) = \frac{32}{\pi^3}\left(\frac{b^2}{2R}\right) \sum_{n\,\mathrm{odd}}^{\infty} \frac{(-1)^{\frac{n-1}{2}}}{n^3} \left[\frac{\cosh\left(\frac{n\pi x}{2\gamma a}\right)}{\cosh\left(\frac{n\pi}{2\gamma}\right)}\right] \cos\left(\frac{n\pi y}{2b}\right) \tag{A8}$$

The solution to problem III is

$$w_{III}(x,y) = \frac{16 b^2 p}{\pi^3 T_y \gamma^2} \sum_{n\,\mathrm{odd}}^{\infty} \frac{(-1)^{\frac{n-1}{2}}}{n^3} \left[1 - \frac{\cosh\left(\frac{n\pi\gamma y}{2b}\right)}{\cosh\left(\frac{n\pi\gamma}{2}\right)}\right] \cos\left(\frac{n\pi x}{2a}\right) \tag{A9}$$

For the square membrane, $a = b$, so that $\gamma^2 = \frac{T_x}{T_y}$; then, defining $W = \frac{a^2}{2R}$, equations (A7) to (A9) combine to yield equations (1) to (3).

Equilateral-Triangular Membrane

For the equilateral-triangular membrane with edges of length L, under isotropic tension T, and with identical symmetric parabolic deflections of magnitude $W = \frac{L^2}{8R}$ on all edges, the deflection shape is

$$w(x,y) = W\left[\frac{8}{9} + \frac{8\sqrt{3}}{3}\frac{x}{L}\left(\frac{x^2}{L^2} - \frac{3y^2}{L^2}\right)\right] \tag{A10}$$

This expression is simply the solution from reference 1 modified to yield zero deflection at the vertices. Accounting for additional deflection due to gravity requires the addition to equation (A10) of the solution to equation (A1), with $T_x = T_y = T$, $p \neq 0$, and $w = 0$ on all edges. This solution is

$$w_g(x,y) = \lambda W\left[\frac{4}{9} - 4\left(\frac{x^2}{L^2} + \frac{y^2}{L^2}\right) - \frac{8\sqrt{3}}{3}\frac{x}{L}\left(\frac{x^2}{L^2} - \frac{3y^2}{L^2}\right)\right] \tag{A11}$$

where $\lambda = \frac{pR}{2T}$. Thus, the total deflection is

$$w(x,y) = W\left[\frac{8}{9} + \frac{4}{9}\lambda - 4\lambda\left(\frac{x^2}{L^2} + \frac{y^2}{L^2}\right) + (1-\lambda)\frac{8\sqrt{3}}{3}\frac{x}{L}\left(\frac{x^2}{L^2} - \frac{3y^2}{L^2}\right)\right] \tag{A12}$$

Reference

1. Fichter, W. B.: Reduction of Root-Mean-Square Error in Faceted Space Antennas. *AIAA J.*, vol. 22, no. 11, Nov. 1984, pp. 1679–1684.

Table 1. Root-Mean-Square Differences for 16-in-Square Facets

Remote tension, lb/in.		δ_1, in.		δ_2, in.			
T_x	T_y	Coarse mesh	Fine mesh	Coarse mesh	Fine mesh	δ_M, in.	δ_F, in.
0.01	0.01	0.013	0.006	0.066	0.056	0.0847	0.1033
		.018	.006	.065	.057		
0.02	0.01	0.013	0.013	0.069	0.064	0.0842	
		.026	.012	.068	.064		
0.02	0.02	0.015	0.013	0.070	0.066	0.0847	
		.022	.013	.070	.066		
0.03	0.01	0.018	0.015	0.073	0.069	0.0833	
		.019	.016	.072	.069		
0.03	0.02	0.030	0.015	0.072	0.069	0.0845	
		.023	.014	.072	.069		

Table 2. Root-Mean-Square Differences for 18-in. Equilateral-Triangular Facets

Remote tension, lb/in.		δ_1, in.		δ_2, in.			
T_x	T_y	Coarse mesh	Fine mesh	Coarse mesh	Fine mesh	δ_M, in.	δ_F, in.
0.01	0.01	0.021	0.007	0.030	0.020	0.0322	0.0633
		.020	.007	.029	.020		
0.02	0.02	0.013	0.014	0.031	0.024		
		.013	.013	.031	.024		
0.03	0.03	0.016	0.015	0.032	0.027		
		.012	.014	.031	.026		

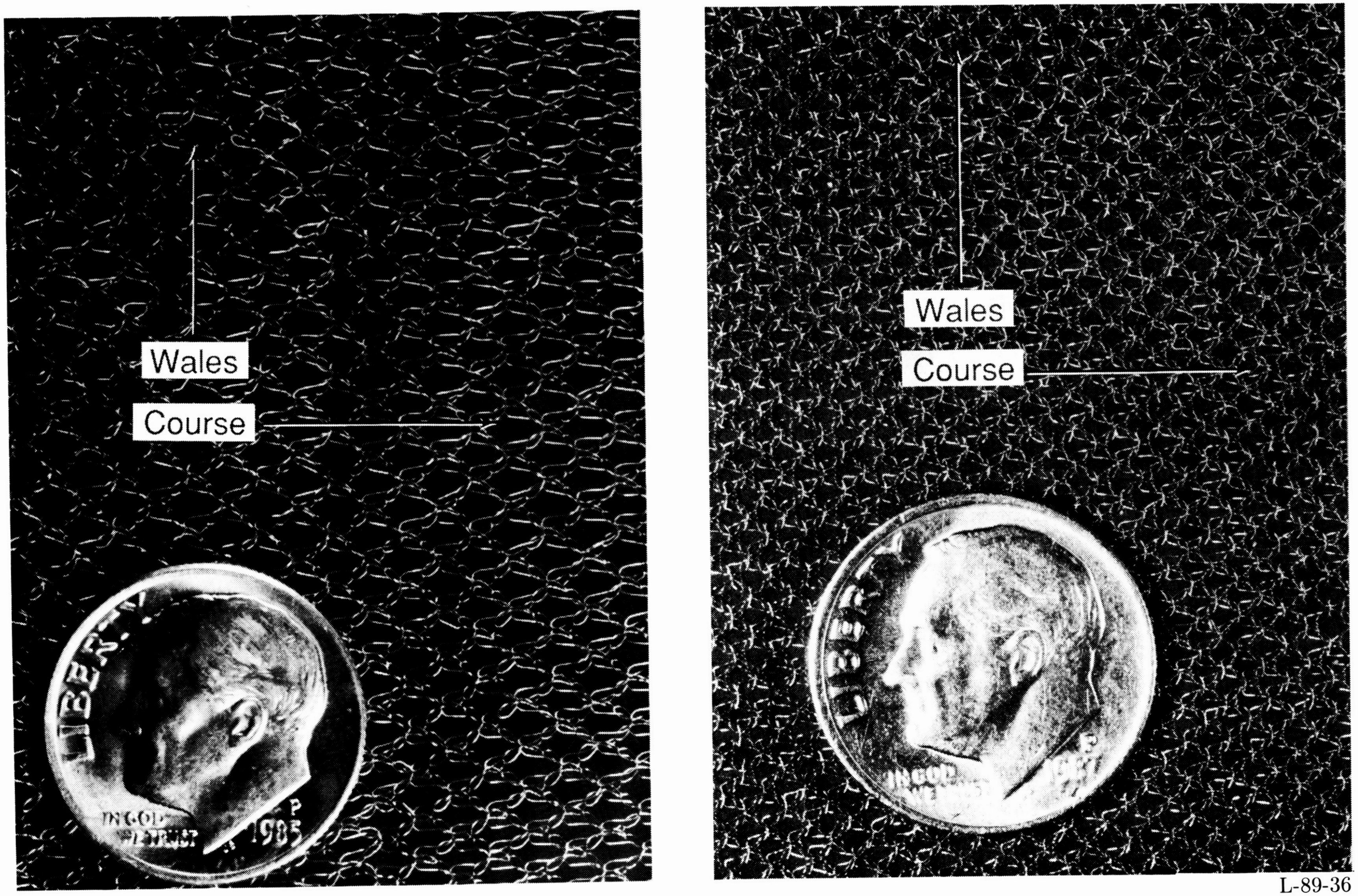

L-89-36

(a) Coarse mesh.

(b) Fine mesh.

Figure 1. Tricot-knit, gold-plated, molybdenum mesh materials.

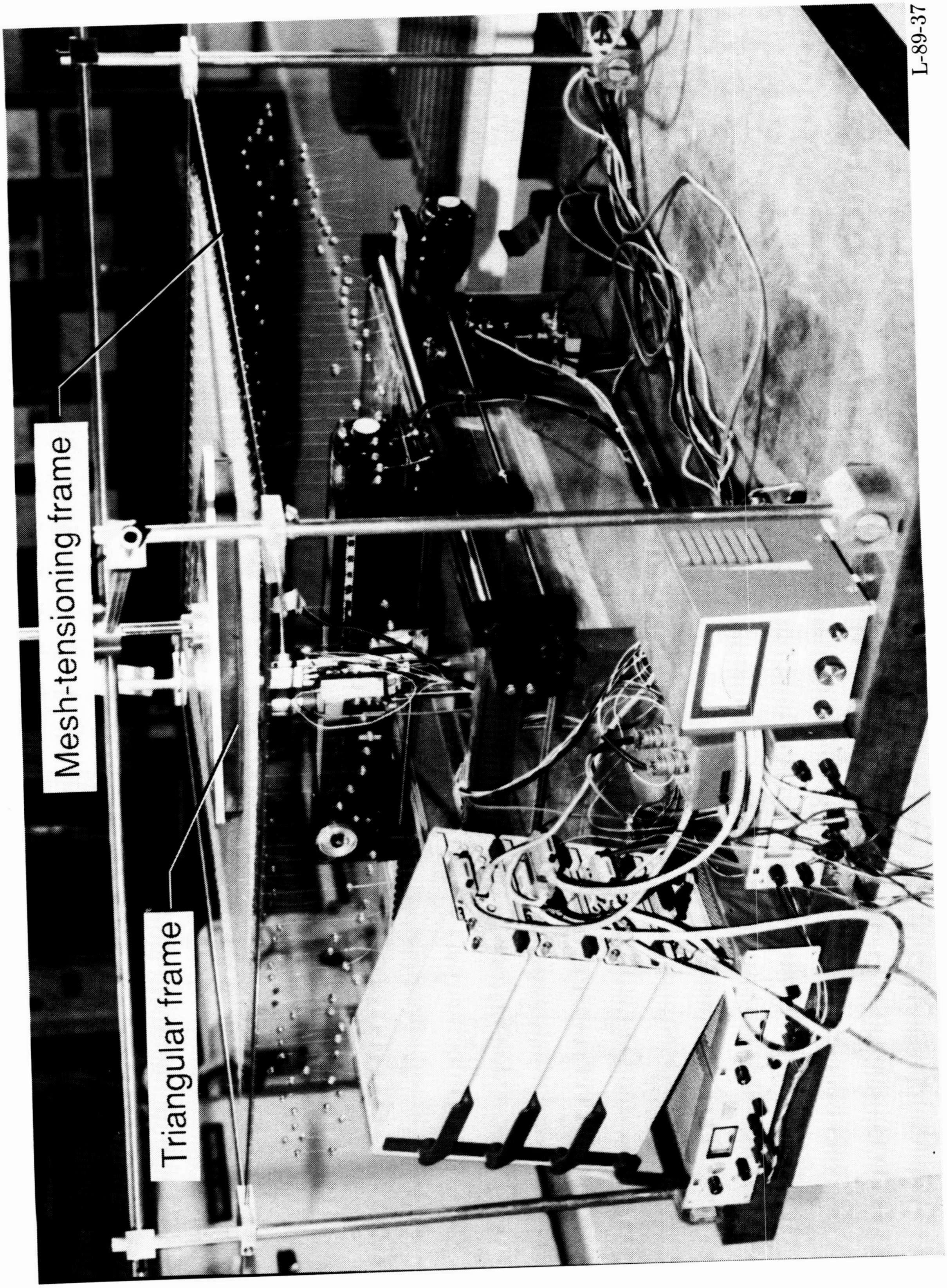

Figure 2. Overall view of test setup.

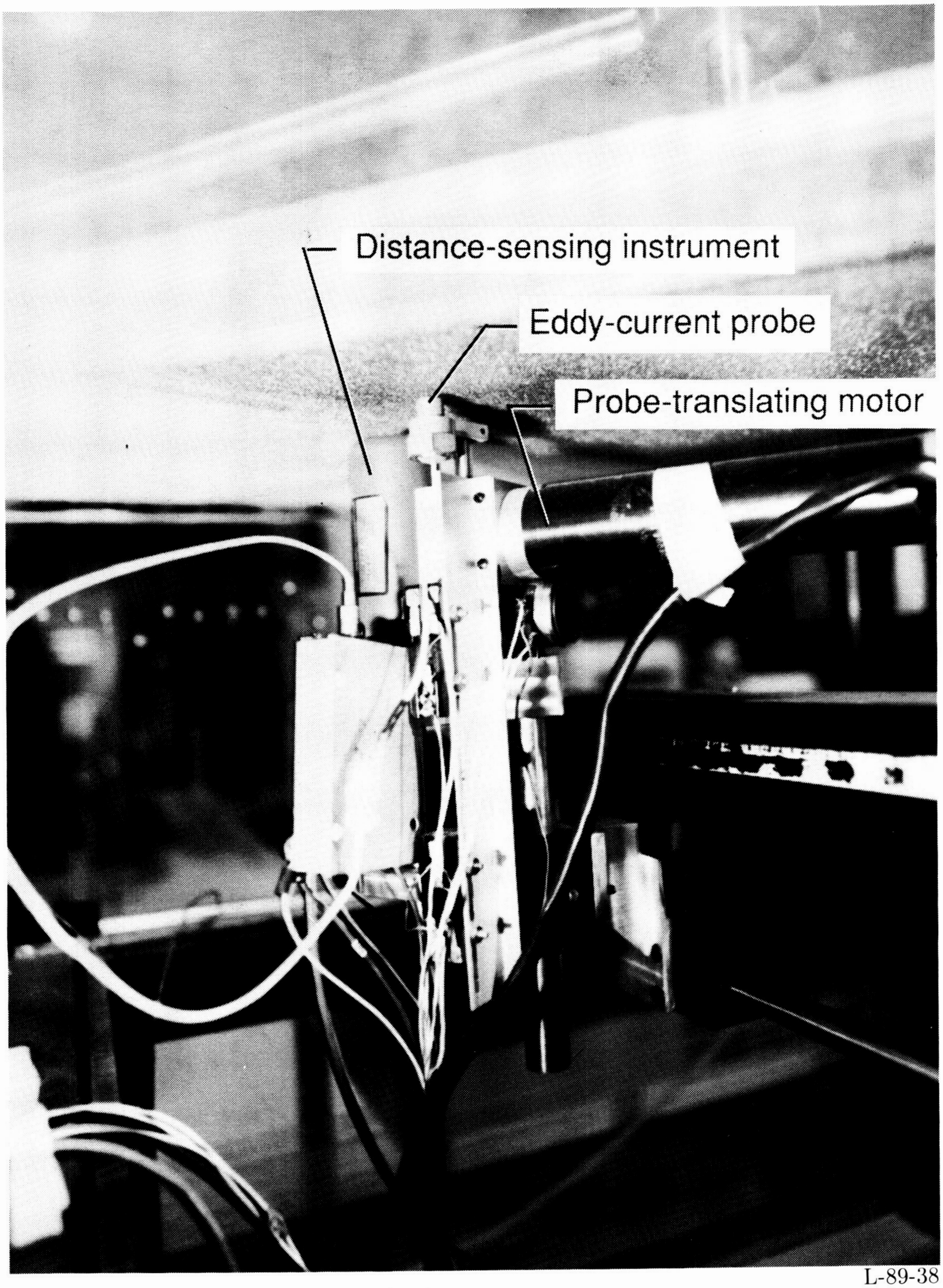

Figure 3. View of deflection-measuring instruments.

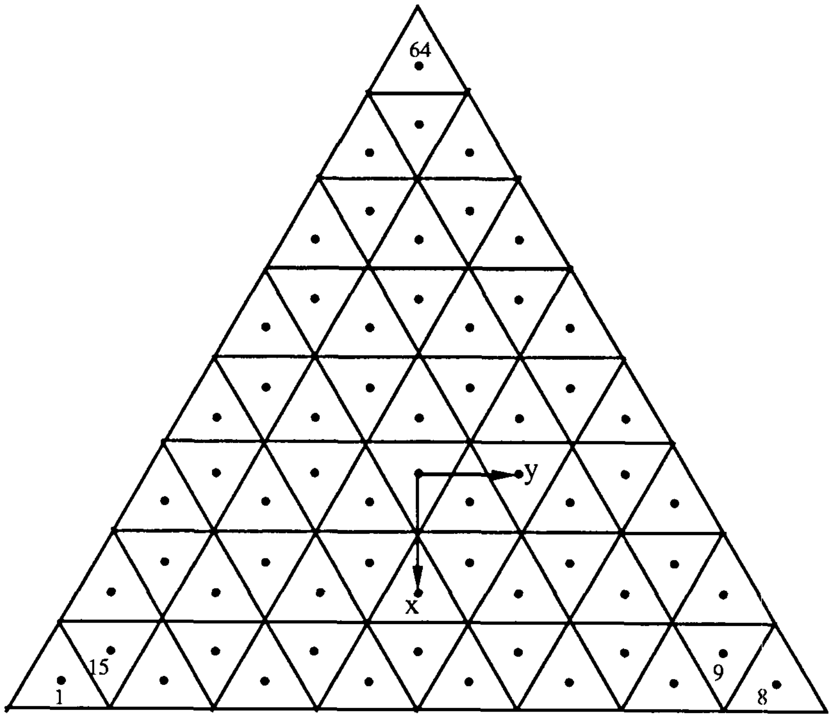

(a) Equilateral triangle.

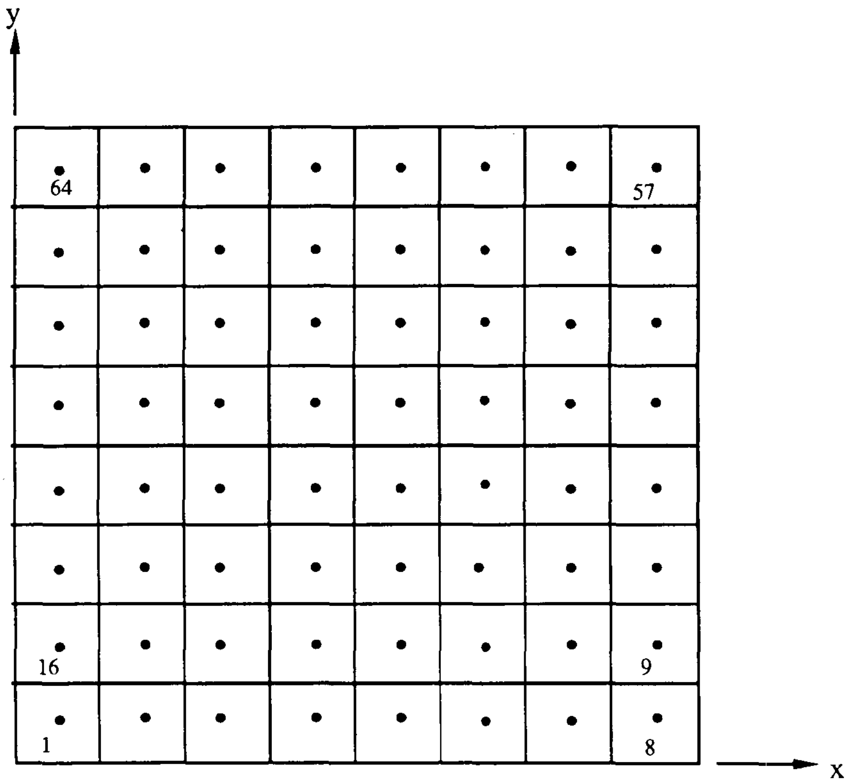

(b) Square.

Figure 4. Coordinate systems and data stations.

National Aeronautics and Space Administration

Report Documentation Page

1. Report No. NASA TP-2896	2. Government Accession No.	3. Recipient's Catalog No.
4. Title and Subtitle Measured and Predicted Root-Mean-Square Errors in Square and Triangular Antenna Mesh Facets		5. Report Date March 1989
		6. Performing Organization Code
7. Author(s) W. B. Fichter		8. Performing Organization Report No. L-16525
9. Performing Organization Name and Address NASA Langley Research Center Hampton, VA 23665-5225		10. Work Unit No. 506-43-41-02
		11. Contract or Grant No.
12. Sponsoring Agency Name and Address National Aeronautics and Space Administration Washington, DC 20546-0001		13. Type of Report and Period Covered Technical Paper
		14. Sponsoring Agency Code

15. Supplementary Notes

16. Abstract

Deflection shapes of square and equilateral-triangular facets of two tricot-knit, gold-plated, molybdenum wire-mesh antenna materials were measured and compared, on the basis of root-mean-square (rms) differences, with deflection shapes predicted by linear membrane theory for several cases of biaxial mesh tension. The two mesh materials contained approximately 10 and 16 holes per lineal inch, measured diagonally with respect to the course and wale directions. The deflection measurement system employed a noncontact eddy-current proximity probe and an electromagnetic distance-sensing probe in conjunction with a precision optical level. Despite experimental uncertainties, rms differences between measured and predicted deflection shapes suggest the following conclusions: (1) replacing flat antenna facets with facets that conform to parabolically curved structural members yields smaller rms surface error; (2) accuracy gains are potentially greater for equilateral-triangular facets than for square facets; (3) linear membrane theory can be a useful tool in the design of tricot-knit wire-mesh antennas.

17. Key Words (Suggested by Authors(s)) Membrane theory Antennas Metallic mesh Root-mean-square error Reflectors		18. Distribution Statement Unclassified—Unlimited Subject Category 39	
19. Security Classif. (of this report) Unclassified	20. Security Classif. (of this page) Unclassified	21. No. of Pages 15	22. Price A03

NASA FORM 1626 OCT 86

NASA-Langley, 1989

For sale by the National Technical Information Service, Springfield, Virginia 22161-2171